

PROCEEDINGS OF SPIE

[SPIDigitalLibrary.org/conference-proceedings-of-spie](https://spiedigitallibrary.org/conference-proceedings-of-spie)

Characterization of the MIRIm double prism assembly at short wavelengths: implications for transit observations of exoplanets

P. Bouchet, R. Gastaud, P.-O. Lagage, S. Kendrew, O. Bombardi, et al.

P. Bouchet, R. Gastaud, P.-O. Lagage, S. Kendrew, O. Bombardi, A. Coulais, S. Ronayette, G. C. Sloan, V. Moreau, T. Orduna, E. Grégoire, A. Dyrek, J. Bouwman, A. Glasse, G. S. Wright, "Characterization of the MIRIm double prism assembly at short wavelengths: implications for transit observations of exoplanets," Proc. SPIE 12180, Space Telescopes and Instrumentation 2022: Optical, Infrared, and Millimeter Wave, 121800Z (27 August 2022); doi: 10.1117/12.2629778

SPIE.

Event: SPIE Astronomical Telescopes + Instrumentation, 2022, Montréal, Québec, Canada

Characterization of the MIRIm double prism assembly at short wavelengths. Implications for Transit Observations of Exoplanets

Bouchet, P.^a, Gastaud, R.^{a,b}, Lagage, P.-O.^a, Kendrew, S.^c, Bombardi, O.^d, Coulais, A.^{e,a}, Ronayette, S.^a, Sloan, G.C.^{f,g}, Moreau, V.^a, Orduna, T.^a, Grégoire, E.^a, Dyrek, A.^a, Bouwman, J.^h, Glasse, A.^{i,j}, and Wright, G. S.^{i,j}

^aUniversité Paris-Saclay, Université Paris Cité, CEA, CNRS, AIM, 91191, Gif-sur-Yvette, France

^bCEA-Saclay, DRF/Irfu/DEDIP, 91191, Gif-sur-Yvette, France

^cEuropean Space Agency, Space Telescope Science Institute, 3700 San Martin Dr., Baltimore, MD 21218, USA

^dPôle Léonard de Vinci, Paris La Défense, France

^eLERMA, Observatoire de Paris, CNRS & Paris Sciences & Lettres University, France

^fSpace Telescope Science Institute, 3700 San Martin Dr., Baltimore, MD 21218, USA

^gDept. of Physics and Astronomy, Univ. of North Carolina, Chapel Hill, USA

^hMax Planck Institute for Astronomy (MPIA), Königstuhl 17, D-69117 Heidelberg, Germany

ⁱUKATC, The Royal Observatory, Blackford Hill, Edinburgh, EH9 3HJ, Scotland

^jInstitute for Astronomy, University of Edinburgh, Royal Observatory, Blackford Hill, Edinburgh EH9 3HJ, Scotland

ABSTRACT

When observing with the slitless Low Resolution Spectroscopic (LRS) mode of the MIRI instrument on board the James Webb Space Telescope (JWST), photons at wavelengths shorter than the nominal wavelength range (5 μm - 12 μm) can reach the detector. In this paper, we study the impact of such photons in terms of opportunity to get spectral information below the nominal cut on, and in terms of possible contamination of the nominal spectrum by those photons. First, we present new laboratory measurements done to characterize the transmission and dispersion of the LRS disperser element, a Double Prisms Assembly (DPA), in the 3-5 μm wavelength range. We confirm a transmission peak at the level of about 30% around 3.7 μm and validate the dispersion optical model. We use the information to simulate how the short wavelengths will impact the spectroscopic images obtained during slitless LRS observations of bright stars; we see a bright spot at the pixel corresponding to the 3.7 μm . Such a spot has indeed been seen in the spectral images obtained during the commissioning of MIRI in May-June 2022; the level of the observed spot is lower than predicted. Such a feature could be useful when observing exoplanets, as it can bring additional information on the exoplanet atmosphere. The effect of spectral contamination is difficult to assess precisely; but, according to the modelisation we did, it is low: at most 7 % in the 5 - 6 μm range and negligible at longer wavelengths.

Keywords: JWST, MIRI, Spectroscopy, InfraRed, exoplanets

1. INTRODUCTION

The Low Resolution Spectroscopic (LRS) mode of the MIRI Imager (MIRIm) produces low-resolution spectra via a Double-Prism Assembly (DPA) which consists of the combination of two prisms, one in Ge and the other one in ZnS, mounted in the MIRI filter wheel. With such a design, the spectral resolution decreases as the

Further author information: (Send correspondence to P.B.)

P.B.: E-mail: patrice.bouchet@cea.fr

Space Telescopes and Instrumentation 2022: Optical, Infrared, and Millimeter Wave, edited by
Laura E. Coyle, Shuji Matsuura, Marshall D. Perrin, Proc. of SPIE Vol. 12180,
121800Z · © 2022 SPIE · 0277-786X · doi: 10.1117/12.2629778

wavelength decreases and varies from a spectral resolving power ($R = \lambda/\Delta\lambda$) of about 40 at 5 μm , to 100 at 7.5 μm , and close to 160 at 10 μm . The LRS offers both slit and slitless spectroscopy from 5 to 12 μm . Spectra are imaged onto the imager detector array.[?] Slitless spectroscopy is only available for time-series observations of time variable phenomena, such as transiting exoplanets or eclipsing binaries, while the LRS slit mode is suited to a broad range of spectroscopic observations. While slitless LRS mode is ideal for high-precision spectrophotometric observations of bright point-source targets, the slit mode gives better performance for faint targets, as background radiation is blocked by the masking structure around the slit.

The dispersion profile folds over below 3.9 μm , superimposing two parts of the spectrum onto each other (see Figure 1). To avoid this contamination a dedicated filter has been mounted over the slit to block radiation shortward of 4.5 μm .[?] This effect is not mitigated for LRS in slitless mode, causing some contamination, but also giving the opportunity to get spectral information shortward the nominal minimum wavelength of 5 μm . The knowledge on the properties of the DPA at wavelengths shorter than 5 μm is limited to a measurement of the transmission at room temperature (see Figure 2) and a theoretical dispersion from the optical model. That is why we decided to use the spare DPA to measure the DPA transmission and dispersion in the 3-5 μm wavelength range at the operating temperature of 7K. The results of these measurements are shown in section 2. In section 3, we have used these measurements to simulate spectral images expected from slitless LRS observations, including wavelengths shorter than 5 microns. Then, in section 4, we compare the simulations with real data obtained during the commissioning of MIRI. In section 5, we discuss the impact of short wavelengths when characterizing the atmosphere of exoplanets and conclude in section 6.

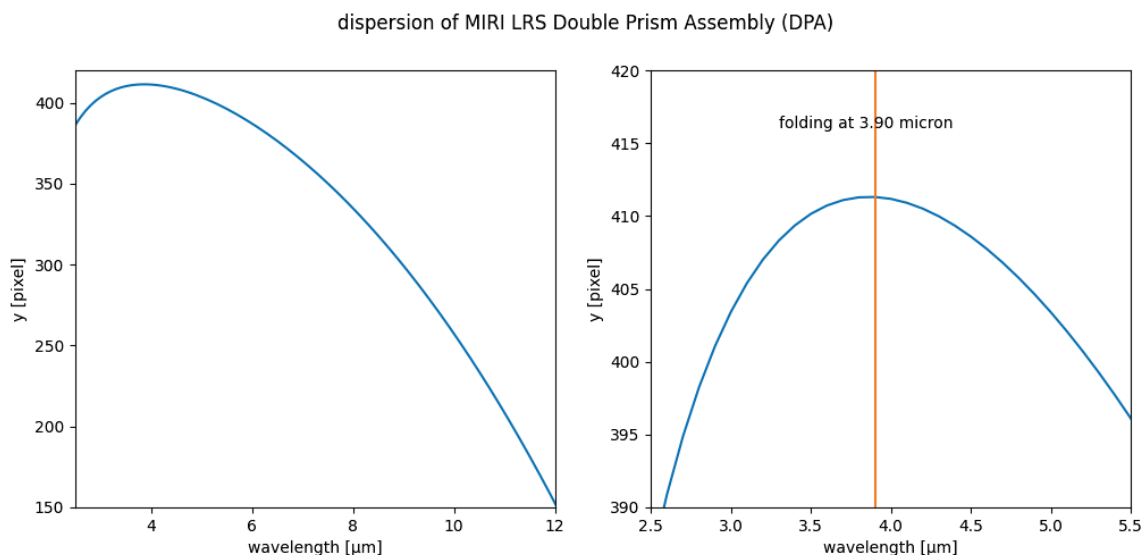


Figure 1. Pixel number where the photons arrive after dispersion by the double prism as a function of wavelength. We can notice that the curve folds at 3.9 μm .

2. LABORATORY MEASUREMENTS

2.1 Test bench

To do a new series of tests, we used the test bench developed at CEA-Saclay to test MIRIm, the imager of MIRI. It consists of : (i) an ambient temperature telescope simulator that includes a JWST-like pupil mask; (ii) an infrared point source with a shutter mounted on a remotely controlled hexapod; (iii) a black body source that can be adjusted between 1150 K and 2000 K, which feeds a monochromator from the Bentham Company, TMc150 type, for which the wavelength calibration accuracy is better than ± 2 nm; (iv) a cryostat containing the engineering model of MIRIm; (v) a focal plane module developed at CEA with a NASA/JPL loaned Sensor Chip

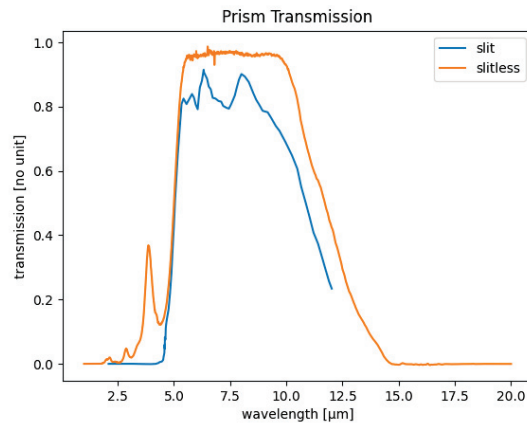


Figure 2. Overall transmissions curves for the LRS double prism (cyan), and for the LRS double prism + slit and filter (blue) (see Kendrew et al. 2015)

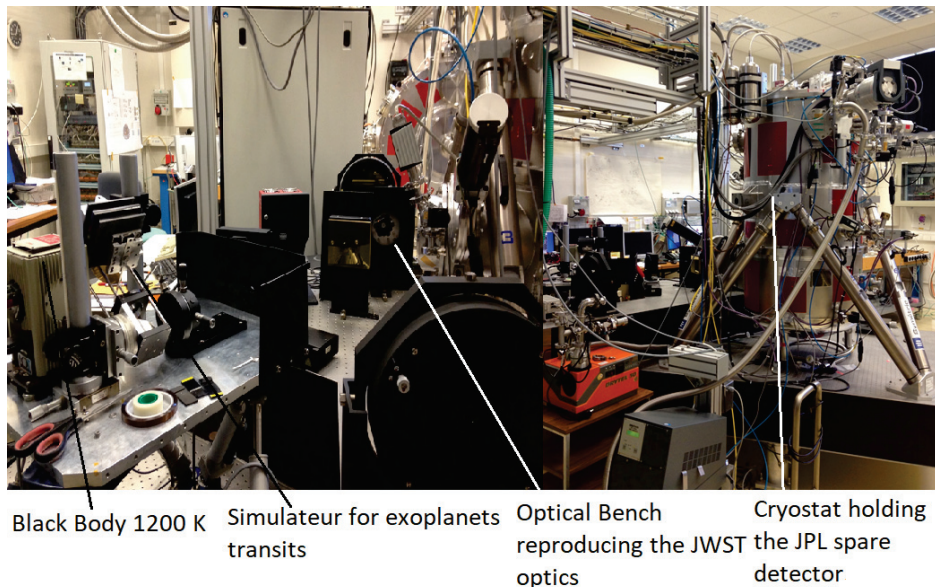


Figure 3. An overview of the MIRI tests bench at CEA-Saclay

Assembly (SCA) fitted with a Raytheon SB305 engineering model of the flight detectors of MIRI. An overview of the tests bench is shown in Figure 3.

2.2 Measurements

We measured the transmission and the dispersion of the DPA at short wavelengths (between 3 and 5 μm) during two series of tests, one in 2018 and the other in 2021. We did the measurements according to the following protocol. A first measurement was done with the DPA in position in the beam. Then we turn the filter wheel and go to the 'hole' position. The ratio of the two signals is proportional to the transmission of the DPA. We scan the wavelength range of interest; the factor of proportionality being independent of the wavelength. The factor of proportionality is obtained by normalizing the measurements in the 5-6 microns range with the transmission curve given by the manufacturer. We used the sub-array on the upper left region of the detector called Slitless mode (see Figure 2 in²). The source diaphragm was set to 75 μm. The monochromator entrance slit was set to 5 mm as we wanted as much flux as possible.

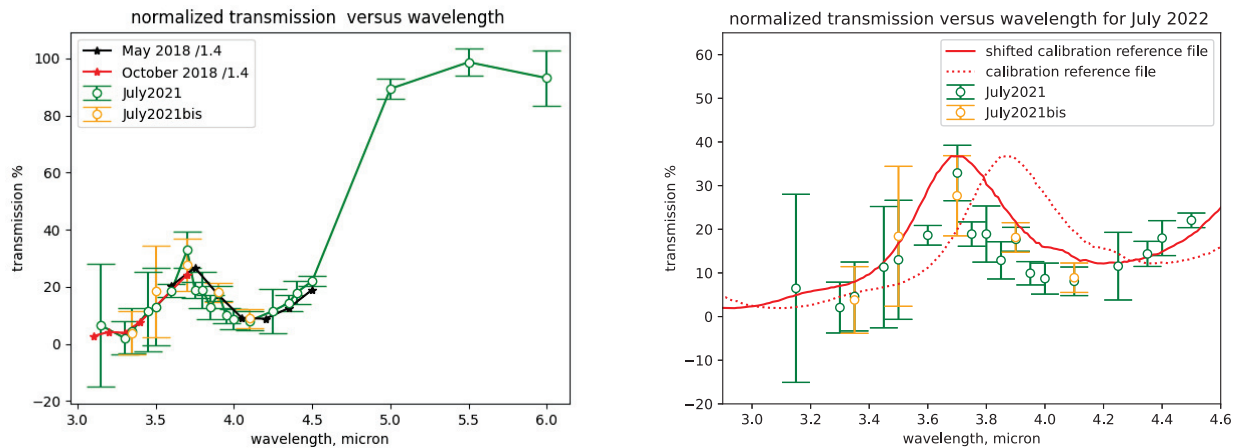


Figure 4. Left : overall transmission observed at Saclay. large wavelength range on the left, zoom in region of interest on the right; the manufacturer curve is in red dot, solid line is the same curve shifted by $0.17 \mu\text{m}$ toward short wavelengths. Error bars are 1σ .

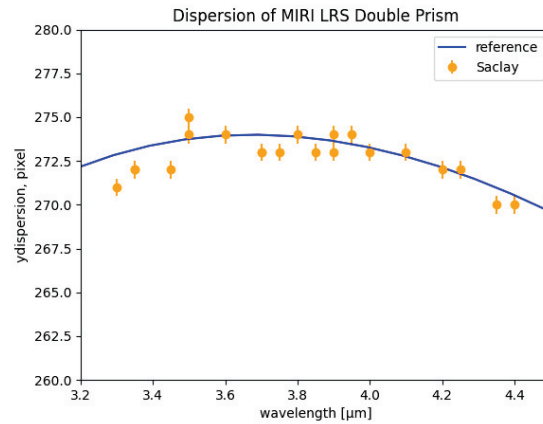


Figure 5. Comparison at wavelength in the $3.3 - 4.5 \mu\text{m}$ range of the optical model dispersion curve with measurements

2.3 Results

Figure 4 shows the measured DPA transmission as a function of the wavelength from the various tests in 2018 and 2021. We confirm that there is a bump in the DPA transmission around $3.7 \mu\text{m}$. The position of the peak varies by $0.05 \mu\text{m}$ between the tests in May 2018 and those in July 2021; we consider that this represents the uncertainty in the wavelength peak of the bump. Note that the bump is shifted by $0.17 \mu\text{m}$ to the short wavelengths when compared to the curve from the manufacturer. This might be due to the difference in operating temperature of the DPA when the measurements are done (ambient for the manufacturer and 7K for the test at Saclay).

We have also measured the dispersion of the DPA at short wavelengths. As shown in Figure 5, the positions on the array of the source as a function of the wavelength fit relatively well with those expected from the optical model. We noticed that the image quality was degraded (see Figure 6). We checked the optical quality with the optical model; and indeed the image quality is degraded as we are pushing the use outside the nominal use (shorter wavelengths and in a corner of the array).

3. SIMULATED SPECTRUM

Having a measurement of the transmission and a validated dispersion curve in the 3- 5 μm , we can extend our simulation to this wavelength range. For the simulation we use a set of 1182 'monochromatic' images provided by the optical model and covering the wavelengths range from 2 to 12.8 μm ; the number of images has been chosen to oversampling the spectral resolution; the images are normalized to 1. We multiply each image by the star flux at the wavelength of the image in photons/m²/ μm /s, then by the telescope collecting area (25 m²), then by the photon-electron conversion factor to go from photons to electrons and then by the difference in wavelength between two adjacent images to get images in e-/s. We co-add all the monochromatic images to get the final simulated image.

The simulated LRS observation of the L168-9 star, a 3800 K star, is shown on Figure 7. We have chosen this star because it has been subject to time series observations during MIRI commissioning. As can be seen the result of the bump in transmission is a bright spot in the image. Although the transmission at the bump is only about 30% of the transmission in the 5 - 12 μm range, the large increase of the star flux with decreasing wavelengths lead to a spot with the brightest pixel.

4. ON-SKY DATA FROM THE COMMISSIONING OF MIRI

The LRS was exercised very thoroughly during the science instrument commissioning period of MIRI,⁷ both in slit and slitless mode. Note that the data unit in the image is Digital Number (DN), while the data unit in the simulated image is electrons (e-/s); to compare the two images, we have applied a conversion factor of 1 e- = 2.5 DN; this value is coherent with the value found during commissioning.

As expected, there is a bright spot at the pixel corresponding to the transmission leak. However the value of the pixel is 50% lower than simulated. The discrepancy might take its origin in a spreading of the Point Spread Function (PSF) due to internal scattering in the detector, effect which is more and more important at lower and lower wavelengths (?) and which has not been taken into account in the simulated images.

We have considered other slitless LRS observations, either obtained with the slitless LRS mode or obtained as by-products of slit observations; (indeed, during a slit observation, slitless spectra of the sources in the field of the imager are obtained). We have extracted a 1D spectrum from the spectral images and calculated the ratio between the maximal value in the nominal wavelength range of 5 - 12 μm and the value observed around 3.7

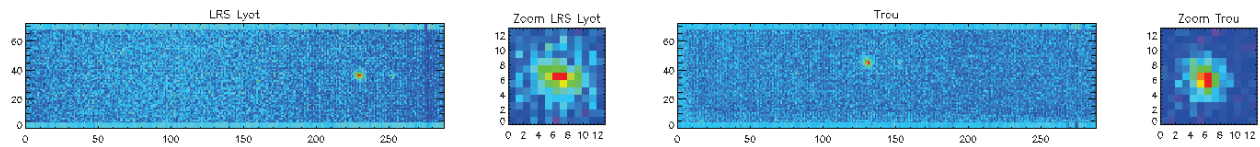


Figure 6. Images at 3.9 μm with DPA (left) and Hole (right). This figure illustrated that, as expected, the image quality is degraded when using the DPA at wavelengths shorter than nominal.

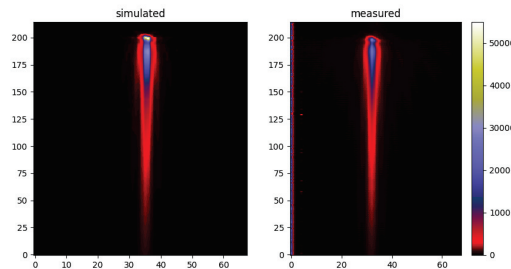


Figure 7. Simulated spectral image of L 168-9 (top) compared with the observed image (bottom); the predicted bright spot at the position of the leak in the DPA transmission at 3.7 μm is observed, but with an intensity lower than expected.

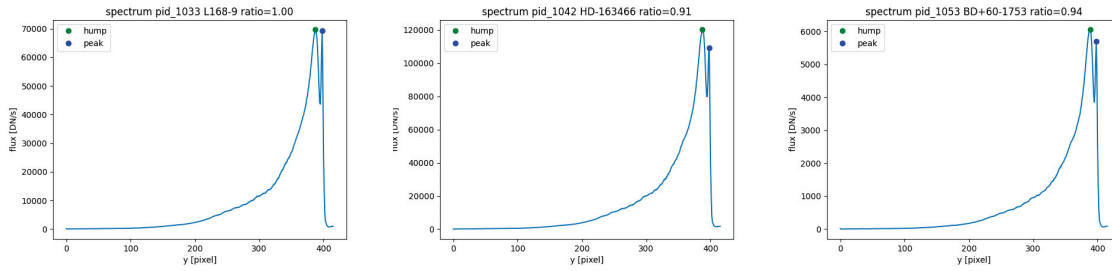


Figure 8. 3 spectra taken with slitless mode from different in-flight data with Program Identity number 1033, 1042, 1053.

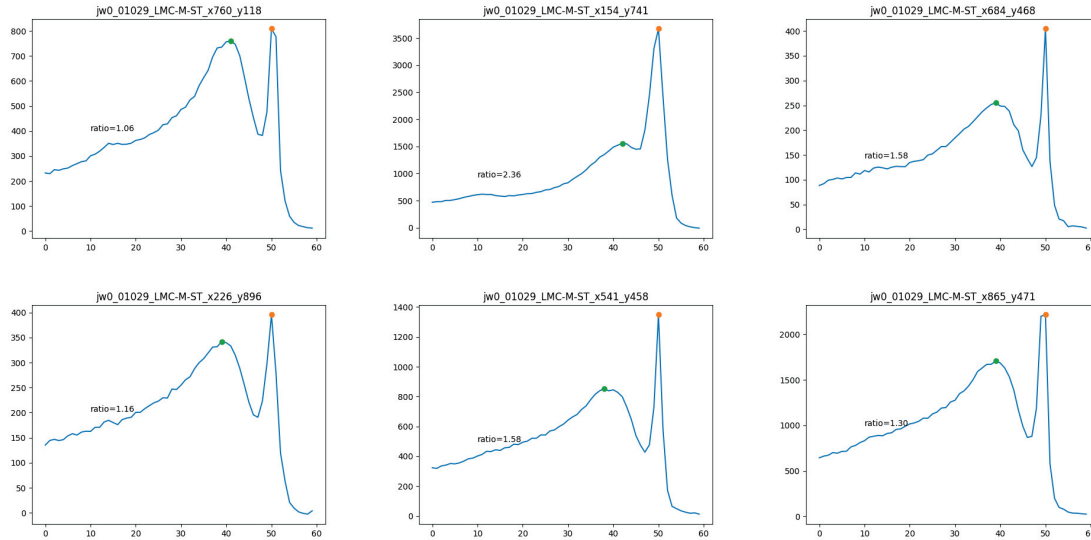


Figure 9. Slitless spectra of six sources in the field of the imager during slit observations (PID 1029; data jw01029007001_03103.00001)

μm (see Figure 8 and Figure 9). The ratio varies between 0.91 and 2.36. The explanation of such a variation is out of the scope of the paper.

5. EXOPLANETS

We have considered whether the transmission ‘leak’ could be useful for exoplanet study. Given that the wavelength of the leak is located near the top of the dispersion curve, the spectral resolution is low; photons with wavelengths between 3.5 and $4.2 \mu\text{m}$ arrive into the same pixel. Around $4 \mu\text{m}$, there are interesting lines of HCN and NH₃ in hot Jupiter atmospheres.[?] A detailed modelisation is needed to study the detectability of those lines from MIRI LRS observations, with the caveat that we have not yet a model which reproduces quantitatively the spectrum around 4 microns, (see section 4).

We have studied another consequence of the particularity of the DPA dispersion curve : the spectral contamination. On figure 10 is shown the % of contamination in the case of transit observations of HAT-P-12b. There are two contamination to consider : the contamination of the spectrum of the star and the one of the planet.

The contamination of the star spectrum has been modeled and is shown in Figure 10. The contamination is only significant in the $5 - 6 \mu\text{m}$ range and is at most of 7 %, again with the same caveat as the one in the previous paragraph. At first order, the contamination of the star is irrelevant when calculating the depth of a transit; indeed the depth is calculated making the difference of flux received out of the transit and during the transit and then normalised by the flux of the star, so that the star contamination doesn’t matter. The previous statement

only hold if the star flux is constant. In general the variability of the star is higher at shorter wavelengths, so that the contamination could introduce some variability.

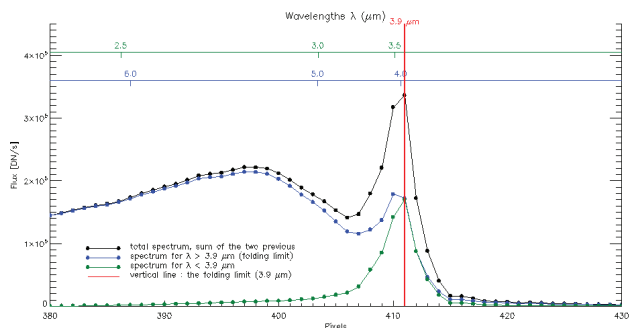


Figure 10. Simulated spectra of HATP-12 showing the effect of contamination; the blue curve is the spectrum without taking into account the wavelengths shorter than $3.9 \mu\text{m}$; the green curve is the spectrum taking only the wavelengths shorter than $3.9 \mu\text{m}$; the black curve is the sum of the two.

The contamination of the exoplanet spectrum depends of course on the exoplanet spectrum at wavelengths shorter than $3.5 \mu\text{m}$, which is in general less steep than the star spectrum, so that we can expect a contamination lower than the one calculated for the star.

6. CONCLUSION

We have performed laboratory measurements to characterize the transmission and dispersion profiles of the double prism assembly (DPA) of the MIRI Low Resolution Spectrometer on JWST, using representative flight spare hardware. Recent measurements in 2021 confirmed previous measurements taken in 2018, and are consistent with the manufacturer’s specifications.

The spectral leak induces a bright spot in the spectrum of a star at about $3.7 \mu\text{m}$, which is close to the turnover in spectral dispersion profile of the DPA. The spot is not currently modeled into the simulation tools for the MIRI LRS in slitless mode, including the Exposure Time Calculator. The bright spot can contain the brightest pixel of the image, which can be saturated. Having such a pixel saturated will not jeopardized the spectrum in the nominal wavelength range. The model we have developed predicts the presence of the spot, but with a value higher than observed.

The spot can potentially be of interest to constraint exoplanet atmosphere. Another aspect of the DPA design is the spectral contamination. The level of contamination of an exoplanet spectrum has been estimated to be limited to the 5 – 6 microns wavelength range and to be of a few % only.

ACKNOWLEDGMENTS

MIRI draws on the scientific and technical expertise of the following organisations: Ames Research Center, USA; Airbus Defence and Space, UK; CEA-Irfu, Saclay, France; Centre Spatial de Liège, Belgium; Consejo Superior de Investigaciones Científicas, Spain; Carl Zeiss Optronics, Germany; Chalmers University of Technology, Sweden; Danish Space Research Institute, Denmark; Dublin Institute for Advanced Studies, Ireland; European Space Agency, Netherlands; ETCA, Belgium; ETH Zurich, Switzerland; Goddard Space Flight Center, USA; Institut d’Astrophysique Spatiale, France; Instituto Nacional de Técnica Aeroespacial, Spain; Institute for Astronomy, Edinburgh, UK; Jet Propulsion Laboratory, USA; Laboratoire d’Astrophysique de Marseille (LAM), France; Leiden University, Netherlands; Lockheed Advanced Technology Center (USA); NOVA Opt-IR group at Dwingeloo, Netherlands; Northrop Grumman, USA; Max-Planck Institut für Astronomie (MPIA), Heidelberg, Germany; Laboratoire d’Etudes Spatiales et d’Instrumentation en Astrophysique (LESIA), France; Paul Scherrer Institut, Switzerland; Raytheon Vision Systems, USA; RUAG Aerospace, Switzerland; Rutherford Appleton

Laboratory (RAL Space), UK; Space Telescope Science Institute, USA; Toegepast Natuurwetenschappelijk Onderzoek (TNO-TPD), Netherlands; UK Astronomy Technology Centre, UK; University College London, UK; University of Amsterdam, Netherlands; University of Arizona, USA; University of Bern, Switzerland; University of Cardiff, UK; University of Cologne, Germany; University of Ghent; University of Groningen, Netherlands; University of Leicester, UK; University of Leuven, Belgium; University of Stockholm, Sweden; Utah We would like to thank the following National and International Funding Agencies for their support of the MIRI development: NASA; ESA; Belgian Science Policy Office; Centre Nationale d'Etudes Spatiales (CNES); Danish National Space Centre; Deutsches Zentrum für Luft- und Raumfahrt (DLR); Enterprise Ireland; Ministerio De Economía y Competividad; Netherlands Research School for Astronomy (NOVA); Netherlands Organisation for Scientific Research (NWO); Science and Technology Facilities Council; Swiss Space Office; Swedish National Space Board; and UK Space Agency.

REFERENCES

- [1] Kendrew, S., Scheithauer, S., Bouchet, P., Amiaux, J., Azzollini, R., Bouwman, J., Chen, C. H., Dubreuil, D., Fischer, S., Glasse, A., Greene, T. P., Lagage, P. O., Lahuis, F., Ronayette, S., Wright, D., and Wright, G. S., "The Mid-Infrared Instrument for the James Webb Space Telescope, IV: The Low-Resolution Spectrometer," *PASP* **127**, 623 (July 2015).
- [2] Ronayette, S., Cavarroc, C., Kendrew, S., Amiaux, J., Auguères, J. L., Bouzat, M., Guillard, P., Moreau, V., Pantin, E., Bouchet, P., Bensalem, A., Orduna, T., Lagage, P. O., Nehme, C., Belu, A., Glasse, A., Baudoz, P., and Dubreuil, D., "Performance verification of the MIRI imager flight model at CEA," in [*Space Telescopes and Instrumentation 2010: Optical, Infrared, and Millimeter Wave*], Oschmann, Jacobus M., J., Clampin, M. C., and MacEwen, H. A., eds., *Society of Photo-Optical Instrumentation Engineers (SPIE) Conference Series* **7731**, 77313N (July 2010).
- [3] Rigby, J. and et al., "Characterization of JWST science performance from commissioning," *arXiv e-prints*, arXiv:2207.05632 (July 2022).
- [4] Gáspár, A., Rieke, G. H., Guillard, P., Dicken, D., Gastaud, R., Alberts, S., Morrison, J., Ressler, M. E., Argyriou, I., and Glasse, A., "The Quantum Efficiency and Diffractive Image Artifacts of Si:As IBC mid-IR Detector Arrays at 5-10 μm : Implications for the JWST/MIRI Detectors," *PASP* **133**, 014504 (Jan. 2021).
- [5] MacDonald, R. J. and Madhusudhan, N., "Signatures of Nitrogen Chemistry in Hot Jupiter Atmospheres," *APJL* **850**, L15 (Nov. 2017).